Solution additives promoting the onset of MgCO₃ nucleation

Dimitrios Toroz,[a] Fu Song,[a] Amira Udin,[a] Greg Chass,*[a,b,c] and Devis Di Tommaso *[a]

[a] Department of Chemistry, Queen Mary University of London, Mile End Road, London, E1 4NS, United Kingdom
[b] Department of Chemistry and Chemical Biology, McMaster University, Hamilton, Ontario, L8S 4M1, Canada
[c] Department of Chemistry, The University of Hong Kong, Pokfulam Road, Hong Kong, P. R. China

Abstract

Formed *via* aqueous carbonation of Mg^{2+} ions, the crystallization of magnesite ($MgCO_3$) is a promising carbon capture and reuse technology, albeit limited by the slow precipitation of $MgCO_3$. Although magnesite is naturally abundant, forming at low temperature conditions, its production is an energy-intensive process due to the temperatures required to prevent the formation of hydrated phases. The principle difficulty arises from the very strong $Mg^{2+}\cdots H_2O$ interaction, raising barriers to dehydration. Using atomistic simulations, we have investigated the influence of thirty additive anions (X^{n-}, $n = 1–3$), ranging from simple halides to more complex molecules, on the first two steps of $MgCO_3$ aggregation from solution: Mg^{2+} dehydration and $Mg^{2+}\cdots CO_3^{2-}$ pairing. We have computed the thermodynamic stability of solvent shared ion pairs, $Mg^{2+}\cdots H_2O\cdots X^{n-}$, and contact ion pairs, $Mg^{2+}\cdots X^{n-}$, with Mg^{2+} to reveal the propensity of solution additives to inhibit $Mg^{2+}\cdots CO_3^{2-}$ formation. We have determined the stabilization of undercoordinated hydrated Mg^{2+} states with a vacant coordination site to which CO_3^{2-} can bind, subsequently initiating $MgCO_3$ nucleation or Mg^{2+} incorporation into the crystal lattice. Extensive molecular dynamics simulations of electrolyte solutions containing Na_2CO_3 with different sources of Mg^{2+}, $MgCl_2$, $MgSO_4$ and $Mg(CH_3COO)_2$, further shows that the degree of dehydration of Mg^{2+} and the structure of prenucleation $MgCO_3$ clusters changes depending on the type counterion. Through a fundamental understanding of the role of solution additives in the mechanism of Mg^{2+} dehydration, our computational study can rationalize previously reported experimental observation of the effect of solvation environments on the growth of magnesite. This understanding may contribute to identifying solution composition conditions that could promote the low-temperature CO_2 conversion into $MgCO_3$.

Keywords: CO_2 mineralization, Mg^{2+} dehydration, magnesium carbonate, molecular dynamics

1. Introduction

Mineralization of carbon dioxide (CO_2) has the benefits of unlimited raw material supplement and longer-term storage carbonate materials, expected to reach $1 trillion per year by 2030.[1] The anhydrous form of magnesium carbonate, magnesite, is a widely used in the food, fertilizer, in manufacture of refractory materials, as a valuable construction material due to its fire-retardant properties, and in the production of eco-cements.[2] Mining of $MgCO_3$ exceeds 25 Mt yr⁻¹ but its deposits are concentrated in Russia, China, and Korea.[3] Conversely, magnesium ion (Mg^{2+}) sources are widespread and plenty (Mg-silicate deposits are 100,000 Gt) [4] and $MgCO_3$ could be produced *via* mineral carbonation of Mg-silicate.[5] However, CO_2 mineralization into $MgCO_3$ is limited by the slow rates of

magnesite precipitation from solution.[5] Its production is an energy-intensive process due to the high temperatures (T = 120–600 °C) required to prevent the formation of hydrated Mg-carbonate phases such as nesquehonite, $MgCO_3 \cdot 3H_2O$, and hydromagnesite, $Mg_5(CO_3)_4(OH)_2 \cdot 4H_2O$.[6] The high T necessary to promote the direct precipitation of anhydrous $MgCO_3$, the increased solid mass and volume of nesquehonite and hydromagnesite per mole of CO_2 sequestered, as well as their inferior mechanical and structural properties, all have negative impacts on the cost, industrial viability, and profitability of CO_2 mineralization.[7] The slow precipitation rate of $MgCO_3$ has long been ascribed to the very strong $Mg^{2+} \cdots H_2O$ interaction (hydration free energy of Mg^{2+} is –439 kcal mol^{-1}),[8] which raises the barrier of Mg^{2+} dehydration.[9]

The solvation environment in which the mineral crystallization occurs may influence the Mg^{2+} dehydration process. In this regard, McKenzey et al. proposed that bisulfide delivered by sulphate reducing bacteria in sedimentary environments could catalyze natural dolomite, $CaMg(CO_3)_2$, formation.[10] To accelerate the synthesis of anhydrous $MgCO_3$ under standard conditions, efforts have focused on the addition of salts,[11,12] complexing compounds,[13] alcohol molecules,[14] and microorganisms.[15] However, there is a lack of a comprehensive study regarding the effects of solution additives in the fundamental processes controlling the Mg^{2+} dehydration process.

We present a computational characterization of the influence of solution additives on the hydration properties of Mg^{2+} to determine which additives may accelerate the Mg^{2+} dehydration and the subsequent steps of $MgCO_3$ nucleation. **Table 1** reports the 30 solution additive ions (X^{n-}, $n = 1–3$) considered in this study: Ions abundant in groundwater such as chloride (Cl^-), fluoride (F^-), sulphate (SO_4^{2-}), nitrate (NO_3^-), phosphates ($H_nPO_4^{3-n}$, $n = 0–2$), silicate (SiO_3^{2-}) as well as (bi)carbonate $(H)CO_3^-$ [16]. Ions that have been deemed important in promoting the formation of anhydrous forms of Mg-carbonates such as bisulfide (HS^-) and carboxylic acids ($HCOO^-$ and CH_3COO^-).[10,13] Molecular ions containing multiple functional groups that may act cooperatively to promote Mg^{2+} dehydration such as taurate ($C_2H_6NSO_3^-$), aspartate ($C_4H_6NO_4^{2-}$), oxalate ($C_2O_4^{2-}$), salicylate ($C_7H_5O_3^-$), citrate ($C_6H_5O_7^{3-}$), tartrate ($C_4H_4O_6^{2-}$), malate ($C_4H_4O_5^{2-}$), and amino phenolate ($C_6H_4ONH_2^-$). Peptides and alcohol molecules considered responsible for facilitating Mg^{2+} dehydration such as glycinate ($C_2H_4NO_2^-$), glutamate ($C_5H_8NO_4^-$), aspartate ($C_4H_6NO_4^{2-}$), and isopropyl alcohol ionic ($C_3H_7O^{2-}$).[14,17–19] Finally, the hexafluorosilicate ion (SiF_6^{2-}) is produced on large scales on volcanoes [20] and has been speculated to accelerate natural $MgCO_3$ formation.[21] Such a computational database may be used to identify conditions of solution compositions catalysing the low-temperature CO_2 conversion into $MgCO_3$.

We have used a combination of atomistic simulation methods, well-tempered metadynamics-biased molecular dynamics (CMμD), to characterize the ability of the solution additive ions in **Table 1** of promoting Mg^{2+} dehydration based on two well defined, molecular level criteria: form solvent shared ion pairs or contact ion pairs with Mg^{2+} that are less stable than $Mg^{2+} \cdots CO_3^{2-}$; stabilize undercoordinated hydrated Mg^{2+} states with with a vacant coordination site to which CO_3^{2-} can bind, initiating the $MgCO_3$ nucleation or the Mg^{2+} incorporation into the crystal lattice. Subsequently, we have conducted unbiased classical molecular dynamics (MD) simulations of $MgCO_3$ aggregation in the presence of selected additives to monitor the effect of solution composition of the dynamics of formation and the structure of prenucleation clusters. By providing a fundamental understanding of how the presence of solution additives can influence the rate-determining Mg^{2+} dehydration step, the composition of the solution might be tuned to accelerate the kinetics of the early stages of $MgCO_3$ nucleation and growth.

2

Table 1. The solution additive ions (X^{n-}) used to assess the effect of solution composition in promoting Mg^{2+} dehydration.

X^{n-}	Formula	Additive ion	Abbreviation
1	Cl^-	Chloride	CL
2	F^-	Fluoride	F
3	I^-	Iodide	I
4	NO_3^-	Nitrate	NO3
5	HCO_3^-	Bicarbonate	HCO3
6	ClO_4^-	Pechlorate	CLO4
7	CO_3^{2-}	Carbonate	CO3
8	SO_4^{2-}	Sulphate	SO4
9	HS^-	Bisulfide	HS
10	$HCOO^-$	Formate	HCOO
11	CH_3COO^-	Acetate	CH3COO
12	PO_4^{3-}	Phosphate	PO4
13	HPO_4^{2-}	Hydrogen phosphate	HPO4
14	$H_2PO_4^-$	Dihydrogen phosphate	H2PO4
15	SiO_3^{2-}	Metasilicate	SIO3
16	$C_2H_6NSO_3^-$	Taurate	TAU
17	$C_2O_4^{2-}$	Oxalate	C2O4
18	$C_7H_5O_3^-$	Salicylate	SAL
19	$C_6H_5O_7^{3-}$	Citrate	CIT
20	$C_4H_6NO_4^{2-}$	Aspartate	ASP
21	$C_4H_4O_6^{2-}$	Tartrate	TAR
22	$C_4H_4O_5^{2-}$	Malate	MAL
23	$C_6H_4ONH_2^-$	Amino phenolate	PHENAM
24	$C_2H_4NO_2^-$	Glycinate	GLY
25	$C_5H_8NO_4^-$	Glutamate	GLU
26	OH^-	Hydroxyl	OH
27	$C_6H_5O^-$	Phenolate	PHEN
28	$C_3H_7O^{2-}$	Isopropyl alcohol ionic	IPA
29	$C_8O_5H_{16}^{2-}$	Polyethylene glycol	PEG
30	SiF_6^{2-}	Hexafluoro Silicate	SIF6

2. Computational details

Classical MD simulations were performed using GROMACS version 2016.3.[22] The leapfrog algorithm with a time step of 2 fs was used to integrate the equations of motion. Simulations were conducted in the isothermal (constant NVT) and isothermal-isobaric (constant NPT) ensemble at the target temperature T = 300 K and pressure P = 1 bar. The velocity rescale thermostat and the isotropic Parrinello-Rahman barostat were used with 0.4 ps and 2.0 ps as the thermostat and barostat relaxation times, respectively. The electrostatic forces were calculated by means of the particle-mesh Edwald approach with a cutoff of 1.2 nm. A 1.2 nm cutoff was also used for the van der Waals forces. The LINCS algorithm was used at each step to preserve the bond lengths. Periodic boundary conditions were applied throughout.

Free energy calculations were conducted computed by means of the well-tempered metadynamics-biased MD (CMµD) method,[23] using GROMACS 2016.3 equipped with the PLUMED 2.4.1 plugin.[24] The distance between Mg^{2+} and the center of mass of the additive was used as collective variable to compute the formation of ion pairs. Two collective variables were used to study the Mg^{2+} dehydration process: Mg^{2+}−water distance; Mg^{2+}−water coordination number (CN). The latter was defined using the continuous differentiable function:

$$CN = \sum_i \frac{1 - \left(\frac{r_i - d_0}{r_0}\right)^n}{1 - \left(\frac{r_i - d_0}{r_0}\right)^m} \tag{1}$$

where $r_0 = 1.1$ Å, $d_0 = 1.9$ Å, $n = 4$, $m = 8$, r_i is the distance between Mg^{2+} and the oxygen atom of i-th water molecule.[25] The free energy profiles were constructed by running CMμD simulations with Gaussians laid every 1 ps and with an initial height equal to k_BT. The Gaussian widths were 0.2 and 0.1 along the distance and coordination number (CN), respectively.[26]

The solution additives were modelled using the General Amber Forcefield (GAFF) [27] to model the additives labelled NO_3^-, SIF_6^- and HS^-, and the AMBER-99 [28] forcefield to model the other molecular ions in **Table 1**. The Mg^{2+}–water interactions were described by the Lennard–Jones GAFF potential together with the SPC/E water model,[29] which we have previously shown to give structural, dynamic and kinetic properties of hydrated Mg^{2+} in good agreement with quantum chemical and experimental data.[9] Moreover, the use of the AMBER class of forcefield has allowed us to simulate the Mg^{2+} dehydration in the presence of other electrolytes using a consistent set of intra- and inter-molecular forcefield parameters. The Antechamber package was used to compute the atomic partial charges in the framework of the restrained electrostatic potential formalism [30] on the optimized structure and electrostatic potential of the molecular ions determined with the Gaussian09 electronic structure code at the HF/6-31G* level of theory.[31]

The following protocol was used to generate the Mg^{2+} containing electrolyte solutions. We first conducted MD (NPT) simulation of around 1400 water molecules for 1 ns to generate an equilibrated aqueous solution. This was used to generate Mg^{2+} / X^{n-} solutions by randomly replacing two water molecules with one magnesium ion and one counterions. We then conducted a series of NVT simulations for $Mg^{2+}\cdots X^{n-}$ separation distances (d) varying from 13 Å to 4.5 Å using a harmonic bias potential with a force constant of 500 kJ.mol⁻¹. Starting from the last configuration corresponding to a $Mg^{2+}\cdots X^n$ distance of approximately 4.5 Å, CMμD simulations were conducted in the NVT ensemble for 100 ns, which we is sufficient to obtain convergent free energy profiles as a function of the Mg^{2+}-water coordination number (**Fig. S1** in Supporting Information). For each of the additives, the free energy profiles are the average of three different repeats. We performed three repeats for all the additives assessed. To evaluate the magnitude of the ability of each additive to promote Mg^{2+} dehydration, we have conducted two further sets of CμMD simulations with respect to Mg^{2+}−water coordination: in the first set the $Mg^{2+}\cdots X^{n-}$ separation was kept at 4.5 Å, which corresponds to the position of the second Mg^{2+} hydration shell, by imposing a harmonic bias potential with a force constant of 1000 kJ.mol⁻¹ along the reaction coordinate defined as the distance between the two ions; in the second set Mg^{2+} and X^{n-} were in direct contact.

3. Results

By influencing the hydration structure of Mg^{2+}, organic ligands and inorganic ions in aqueous environments may activate the Mg^{2+} dehydration.[32] In solution, interacting Mg^{2+} and X^{n-} could be in direct contact or intervened by a water molecule. These states are labelled, respectively, contact ion pair (CIP) and solvent-separated ion pair (SSIP) states.[33] Ion pairs with a single water molecule intervening the ions are also sometimes called solvent-

shared ion pairs (SSHIP).[34] The tendency of the magnesium and additive ions to form contact or solvent-separated pairs depends on the competition between $Mg^{2+}\cdots H_2O$ and $Mg^{2+}\cdots X^{n-}$ interactions. We have quantified the strength of ion paring in terms of the free energy as a function of the $Mg^{2+}\cdots X^{n-}$ distance (**Fig. 1a**). In the initial configuration, the Mg^{2+} and the counterion were separated by at least 0.4 nm and CMμD was then been applied to compute the free energy profiles over separation distances up to 0.8 nm and determine which Mg^{2+} / X^{n-} pair form a thermodynamically stable contact ion. Key features of these profiles are summarized in **Table 2**, where the standard Gibbs energy of activation ($\Delta^{\ddagger}G$) and Gibbs free energy of reaction (ΔG) are given with respect to the free energy of the SSHIP at approximately 0.45 nm of each Mg–X pair. The free energy for the removal of a water molecule from the first hydration shell of Mg^{2+} has also been computed to determine if a particular $Mg^{2+}\cdots X^{n-}$ contact ion pair is thermodynamically more stable than the hexa-hydrated complex $[Mg(H_2O)_6]^{2+}$. For example, the free energy for the $Mg^{2+}\cdots CO_3^{2-}$ pairing (ΔG = –26 kJ.mol–1) are significantly lower than $[Mg(H_2O)_6]^{2+}$ (–7 kJ.mol^{-1}), whilst the Gibbs energy of activation of these CIPs are lower than $Mg^{2+}\cdots H_2O$ dissociation ($\Delta^{\ddagger}G$ = +48 kJ.mol^{-1}). Consequently, the $Mg^{2+}\cdots CO_3^{2-}$ CIP should be thermodynamically and kinetically favorable compared to $[Mg(H_2O)_6]^{2+}$.

Table 2. Positions and free energies of formation of the contact (CIP) and solvent shared (SSHIP) Mg^{2+} / X^{n+} ion pairs computed from CMμD simulations as a function of $Mg^{2+}\cdots X^{n+}$ internuclear distance. The values of r_1^{min} and r_2^{min} refer to the position of the CIP and SSHIP on the free energy profile, and the value of r^{max} to the position of the transition state between CIP and SSHIP. The Gibbs free energies of reaction (ΔG) and standard Gibbs energy of activation ($\Delta^{\ddagger}G$) are with respect to SSHIP. The values are compared with those obtained for the removal of a single water molecule from hydrated Mg^{2+}. Distances in nm and free energies in kJ.mol^{-1}.

Additive	r_1^{min}	r^{max}	r_2^{min}	ΔG	$\Delta^{\ddagger}G$
PO4	0.176	-	-	–111.0	-
HCO3	0.191	0.394	0.254	–4.2	55.2
HCOO	0.191	0.387	0.254	–1.7	42.7
NO3	-	0.792	-	-	-
SIO3	0.189	0.351	0.266	–47.8	54.6
CO3	0.188	0.336	0.259	–42.7	25.0
HPO4	0.187	0.399	0.272	–54.4	40.0
PEG	0.187	0.370	0.264	–52.3	48.8
IPA	0.187	0.363	0.271	–49.2	49.9
OH	0.183	0.367	0.261	–51.9	52.1
PHEN	0.190	0.430	0.275	–39.8	45.3
SO4	0.190	0.401	0.260	–29.0	44.7
MAL	0.190	0.372	0.253	–16.7	38.5
C2O4	0.190	0.380	0.253	–23.5	30.8
H2PO4	0.193	0.411	0.270	–31.6	52.7
PHENAM	0.190	0.416	0.275	–41.2	47.5
SIF6	0.192	0.417	0.255	–0.6	20.1
CIT	0.189	0.407	0.266	–43.6	41.2
ASP	0.190	0.410	0.267	–34.3	51.9
TAU	0.193	0.411	0.277	–18.6	47.7
GLU	0.191	0.388	0.261	–23.6	47.4
GLY	0.190	0.374	0.254	–18.5	36.6
SAL	0.191	0.367	0.255	–16.9	37.6
TAR	0.190	0.373	0.253	–11.0	44.5
CH3COO	0.190	0.380	0.253	–15.7	42.0
HS	0.215	0.398	0.292	–12.1	58.4
F	0.184	0.409	0.261	–62.8	47.0
CLO4	0.202	0.428	0.287	–7.9	36.1
Cl	-	0.475	-	-	-
I	-	0.481	-	-	-
H2O	0.200	0.426	0.292	-11.9	43.5
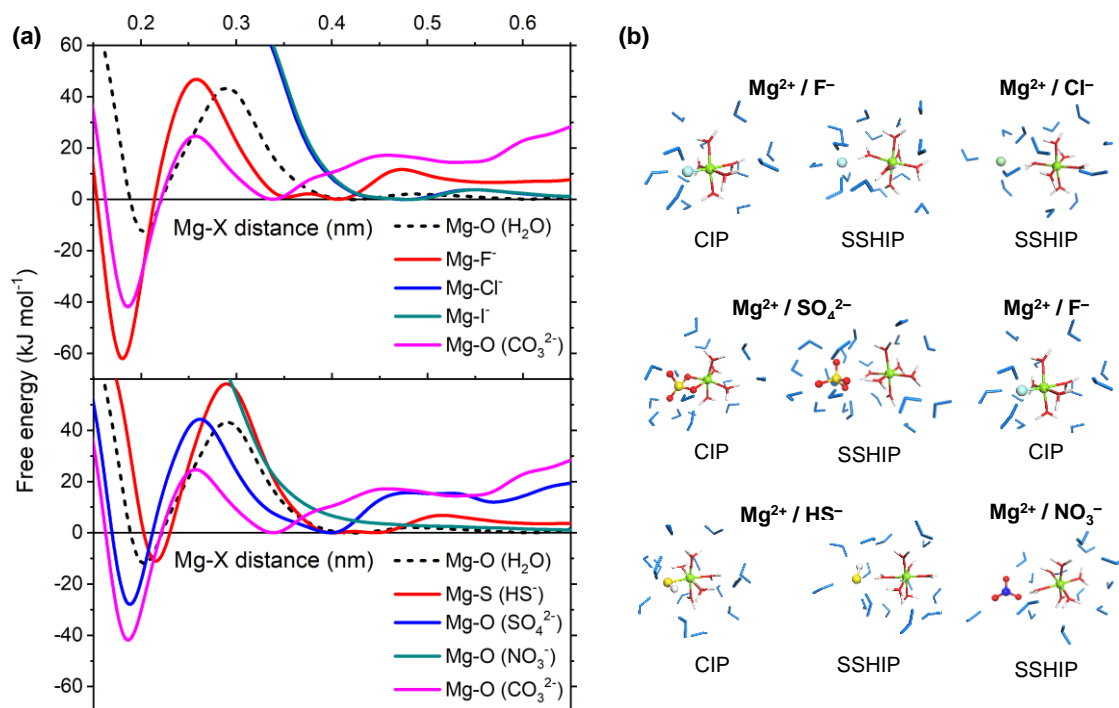
Figure 1. (a) The free energy as a function of the distance between Mg^{2+} and the center of mass of selected solution additive ions ($X^{n-} = F^-, Cl^-, I^-, HS^-, SO_4^{2-}, NO_3^-$). The profiles are compared with the free energy for the removal of a single water molecule from the first hydration shell of $Mg(H_2O)_6^{2+}$. **(b)** Structures of selected contact ion pairs (CIP) and solvent-share ion pairs (SSHIP) corresponding to the minima on the free energy profiles

The structures of the CIP and SSHIP of Mg^{2+} with selected counterions corresponding to the minima on the free energy profiles are reported in **Fig. 1b**. For example, the fluoride ion forms a very stable CIP with Mg^{2+} ($\Delta G = -63$ kJ mol^{-1}). The activation barrier for the formation of $Mg^{2+}\cdots F^-$ ($\Delta^{\ddagger}G = 47$ kJ mol^{-1}) is higher than the free energy necessary to remove a water molecule from $[Mg(H_2O)_6]^{2+}$ ($\Delta^{\ddagger}G = 44$ kJ mol^{-1}). For Cl^-, I^-, and NO_3^{2-} the absence of a free energy minimum on the free energy profile corresponds to the absence of a contact ion pair. In both cases, no disturbance in the Mg^{2+} inner hydration shell is seen priory to the energetically costly replacement of a water molecules with one chlorine, iodide, or oxygen (nitrate). Therefore, Cl^-, I^-, and NO_3^{2-} have the tendency to form solvent-shared pairs ($Mg^{2+}\cdots H_2O\cdots Cl^-$, $Mg^{2+}\cdots H_2O\cdots I^-$, and $Mg^{2+}\cdots H_2O\cdots NO_3^-$) with the magnesium ion. Our results confirm recent broadband dielectric relaxation spectroscopy measurements of aqueous $MgCl_2$ solutions, which show no evidence for the significant formation of CIP.[35] The dominant building unit in the magnesium sulphate solution, $Mg(\eta^2\text{-}SO_4)(H_2O)_4^{2+}$, is reported in **Fig. 1b**: the sulphate coordinates Mg^{2+} in a bidentate mode, the hydration number is four, a result which agrees with static density functional theory calculations of hydrated $MgSO_4$ cluster.[36] The free energy profiles with the sulphate ion show a strong energy minimum corresponding to the formation of $Mg(\eta^2\text{-}SO_4)(H_2O)_4^{2+}$, which is thermodynamically more stable than the $Mg^{2+}\cdots H_2O\cdots SO_4^{2-}$ SSHIP and the hexa-hydrated magnesium complex (**Table 1**). The activation energy of the formation of $Mg^{2+}\text{-}SO_4^{2-}$ ($\Delta^{\ddagger}G = +45$ kJ mol^{-1}) is higher than $Mg\text{-}H_2O$ dissociation (**Table 1**). The CIP with HS^- has similar stability than $[Mg(H_2O)_6]^{2+}$ but the activation barrier of $Mg^{2+}\cdots HS^-$ formation is significantly higher than the free energy necessary for the removal of a water molecule.

Fig. 2 reports the distribution of CIP, SSHIP and SSIP of Mg^{2+} with the additive anions obtained from the analysis of the CMμD simulations, where we have sorted the solution additives according to their ability to form
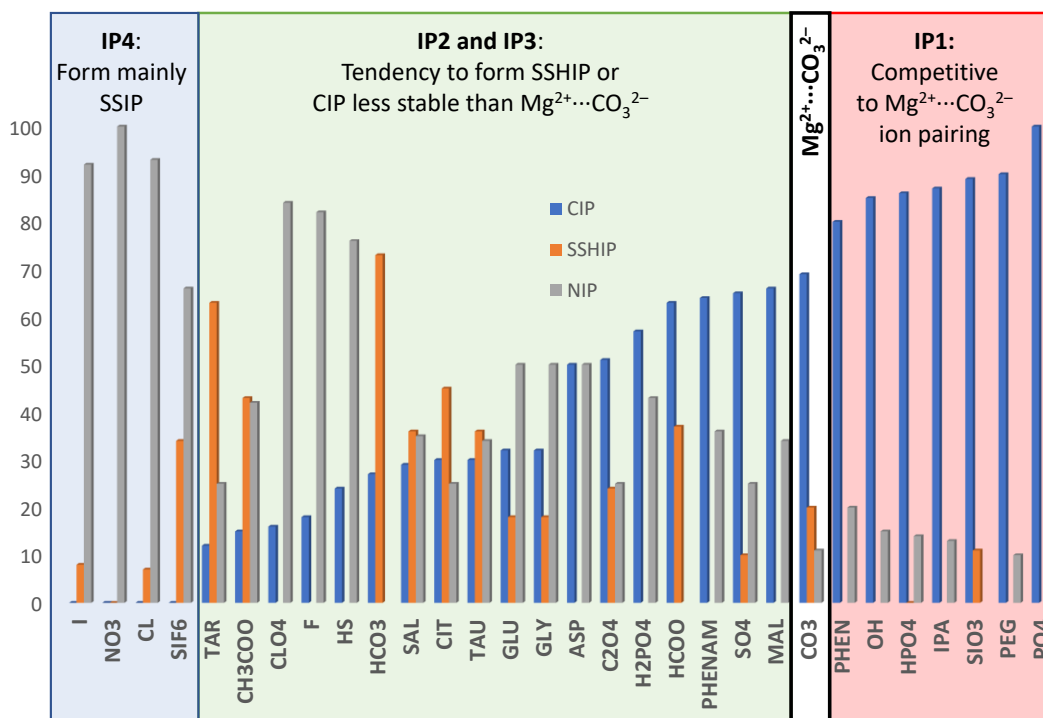
Figure 2. Distribution of contact ion pairs (CIP), solvent shared ion pairs (SSHIP), and solvent separated ion pairs (SSIP) between Mg^{2+} and X^{n-} obtained from the analysis of the CμMD simulations of Mg^{2+} containing electrolyte solutions.

CIPs. Another important aspect to consider is the ability to compete with the formation of $Mg^{2+}\cdots CO_3^{2-}$, the building unit of magnesite. Based on the propensity to form CIPs, SSHIPs or SSIPs, and to inhibit $Mg^{2+}\cdots CO_3^{2-}$ pairing, we have classified the additives anions to the following ion pairing (IP) categories:

IP1: PO4, PEG, SIO3, IPA, HPO4, OH, PHEN. These ions form CIPs that are thermodynamically more stable than $[Mg(H_2O)_6]^{2+}$ and $MgCO_3$ (higher distribution of CIP compared to CO3). Since the ion pairing of $Mg^{2+}\cdots X^{n-}$ is competitive to $Mg^{2+}\cdots CO_3^{2-}$, ions belonging to IP1 may inhibit the early stages of magnesite nucleation.

IP2: MAL, SO4, PHENAM, HCOO, H2PO4, ASP, GLY, GLU, TAU, CIT, SAL, HCO3, F, ClO4, C2O4. These ions form stable CIPs compared to $[Mg(H_2O)_6]^{2+}$ but without being competitive towards $MgCO_3$ pairing (lower distribution of CIP compared to CO3). These ions may promote Mg^{2+} dehydration without inhibiting the early stages of $MgCO_3$ nucleation.

IP3: HS, CH3COO. These ions form stable SSHIP and tend to be in the second hydration shell of Mg^{2+}. While not directly promoting Mg^{2+} dehydration through the formation of more stable CIP than $[Mg(H_2O)_6]^{2+}$, ions of type IP3 may perturb the hydrated Mg^{2+} coordination . Moreover, it is unlikely that HS, CH3COO will inhibit the early stages of $MgCO_3$ nucleation.

IP4: I, CL, NO3, SIF6. These ions are mainly located outside the second hydration shell of Mg^{2+}. Consequently, they show no or little ability to form contact or solvent shared ion pairs. An example is NO3. This ion forms only solvent separated ion pairing and is unlikely to influence the Mg^{2+} dehydration process.

The process of Mg^{2+} dehydration proceeds to a dissociative step [37] and requires the formation of undercoordinated five-hydration intermediates, $Mg(H_2O)_5^{2+}$. We have characterized the influence of counterions on the stabilization of undercoordinated Mg^{2+} states by computing the free energy profile as a function of the

7
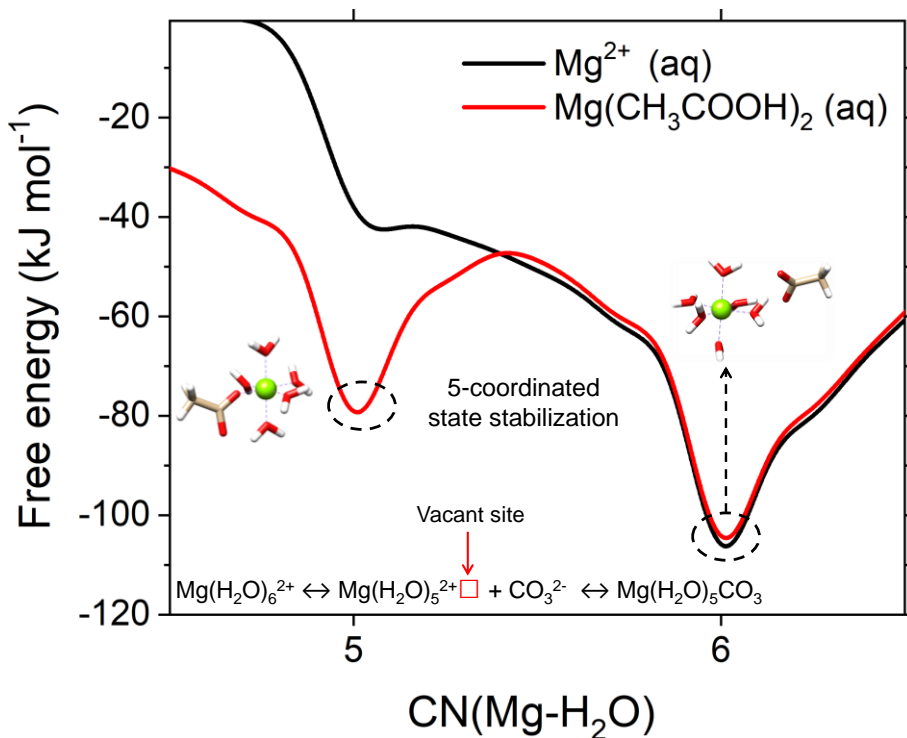
Figure 3. Free energy profiles of hydrated Mg^{2+} as a function of the ion-water coordination number obtained from metadynamics simulations at T = 300K.

number of H_2O molecules in the first hydration shell of the ion, which corresponds to the Mg^{2+}–water coordination number (CN). The Gibbs free energy difference ($\Delta G_{i \to j}$) and free energy barrier ($\Delta^{\ddagger}G_{i \to j}$) between two coordination states i and j may give information on the transition between under- and over-coordinated states during the dynamics of Mg^{2+} (de)solvation [38]. In **Fig. 3**, results of metadynamics simulations of hydrated Mg^{2+} show that in pure liquid water the six-fold coordination with water, $Mg(H_2O)_6^{2+}$, is the most stable hydration state of Mg^{2+}. The generation of a vacant site at the central magnesium ion corresponds to the transformation from the six- to the five-coordinated states to which carbonate can bind to initiate the $MgCO_3$ nucleation or Mg^{2+} incorporation into the magnesite crystal lattice. However, the $Mg(H_2O)_6^{2+} \leftrightarrow Mg(H_2O)_5^{2+}$ conversion is restricted by the high free energy barrier ($\Delta^{\ddagger}G_{i \to j} = 65$ kJ mol^{-1}). Conditions stabilizing the five-coordinated state will promote the Mg^{2+} dehydration process (**Fig. 3**). Mergelsberg recently proposed that the greater salinity in natural systems may stabilize the five-coordinated intermediate.[39] Similarly, the faster kinetics of $MgCO_3$ precipitation measured within the nanoconfined water environments, compared to the bulk solution, was explained in terms of the reduction in coordinating water molecules (fewer than six) for Mg^{2+}.[40]

To quantify the ability of each additive in **Table 1** to promote the Mg^{2+} dehydration process, we have conducted CµMD simulations of electrolyte solutions where the separation between Mg^{2+} and X^{n-} was kept at approximately 4.5 nm by imposing a harmonic potential with a force constant of 1000 kJ.mol^{-1} between the magnesium and the counterion ion. This corresponds to the formation of SSHIP and allows us to evaluate the ability of solution additives to stabilize the undercoordinated Mg^{2+} states. **Fig. 3** shows that the presence of the acetate ion (CH_3COO^-) greatly stabilizes the five-coordinated Mg^{2+} state, promoting its dehydration. Power and co-workers proposed that the Mg^{2+} dehydration by surface-bound carboxyl groups promotes the low-T precipitation of dolomite on carboxylated polystyrene spheres.[41] Therefore, our study demonstrates that at room

8

temperature the presence of specific solutions additives can stabilize under-coordinated complexes, promoting the subsequent steps of Mg-carbonates nucleation and growth.

The ability of additives to replace water molecules when they form SSHIP with Mg^{2+} may accelerate the nucleation events by increasing the proportion of undercoordinated Mg^{2+} species without being competitive to $MgCO_3$ ion pairing. The free energy profiles as a function of the Mg^{2+}-H_2O coordination number, $CN(Mg-H_2O)$, for solvated Mg^{2+} with a counterion in its second hydration shell (solvent-shared ion pairs, SSHIP) are reported in **Fig. 4a**, from which we have extracted the values of the free energies of the four, $[Mg(H_2O)_4]^{2+}$, five, $[Mg(H_2O)_5]^{2+}$, and six, $[Mg(H_2O)_6]^{2+}$, coordination states of Mg^{2+} in solutions containing X^{n-} forming SSHIP with Mg^{2+}. We have identified the following subsets of additives based on the propensity of a counterion to stabilize undercoordinated (four- and five) states with respect to $Mg(H_2O)_6^{2+}$ (**Fig. 4b**), which promotes dehydration even when they form solvent-shared ion pairs (D-SSH).

D1-SSH: PEG, CIT, IPA, PHENAM, C2O4, HCO3. These ions highly stabilize the five-coordination state, which becomes thermodynamically preferred than $Mg(H_2O)_6^{2+}$. We can observe the appearance of a minimum on the free energy profile that corresponds to a tetra-hydrated complex, $Mg(H_2O)_4^{2+}$ (**Fig. 4a**). PEG and IPA are, however, highly competitive to $Mg^{2+}\cdots CO_3^{2-}$ pairing (**Fig. 2**). This class of ions could inhibit the early stages of aqueous magnesite formation.

D2-SSH: SAL, GLU, GLY, TAR, MAL, H2PO4, ASP, OH, HPO4, HCOO, TAU, SIF6, CH3COO, SO4, F, HS. The presence of one of these ions in the second hydration shell of Mg^{2+} leads to a statistically significant stabilization (outside the error bars) of the five-coordination state compared with Mg^{2+} in pure liquid water. However, OH and HPO4 tend to form competitive CIPs to $Mg^{2+}\cdots CO_3^{2-}$ pairing, and SIF6 form mainly solvent separated ion pairs. Otherwise, all other ions can be considered as suitable to dehydrate magnesium.

D3-SSH: SIO3, PHEN, I, CL, CLO4, NO3. In the presence of these ions, the free energy difference between the five and six coordination states, $\Delta G_{5\rightarrow 6}$, is close to that to that in pure water. These ions have, therefore, very little effect on the dehydration of Mg^{2+} and unlikely to promote the early stages of $MgCO_3$ aggregation.

A similar analysis conducted for the solvated Mg^{2+} with a counterion in its first hydration shell (**Fig. S2**) shows the stabilization of states with only three and four water molecules coordinated to Mg^{2+}. However, such a situation would lead to a reaction pathway where the formation of the building unit of magnesite would require the CO_3^{2-} to exchange with the counterion to form the building unit of magnesite: $Mg^{2+}\cdots X^{n-} \rightarrow Mg^{2+}\cdots CO_3^{2-} + X^{n-}$. For this reaction to be thermodynamically possible, the $Mg^{2+}\cdots X^{n-}$ CIP must be less stable than the $Mg^{2+}\cdots CO_3^{2-}$ CIP, which occurs for an additive belonging to **IP2**, **IP3** and **IP4** according to the ion pair distribution analysis. We have identified the following subsets of additives based on the propensity of a counterion in the first hydration shell of Mg^{2+} to stabilize undercoordinated (three- and four) states (D-CIP):

D-CIP1: PO4, HPO4 and H2PO4 and CO3. The most stable hydrated states of Mg^{2+} when coordinated with these ions has only three water molecules. However, PO4 and HPO4 form more stable CIP with Mg^{2+} than the carbonate ion.

D-CIP2: PHENAM, TAR, PEG, MAL, CIT, C2O4 and SO4. The most stable hydrated states of Mg^{2+} when coordinated with these ions has fours water molecules. Moreover, these ions are less competitive than $Mg^{2+}\cdots CO_3^{2-}$.
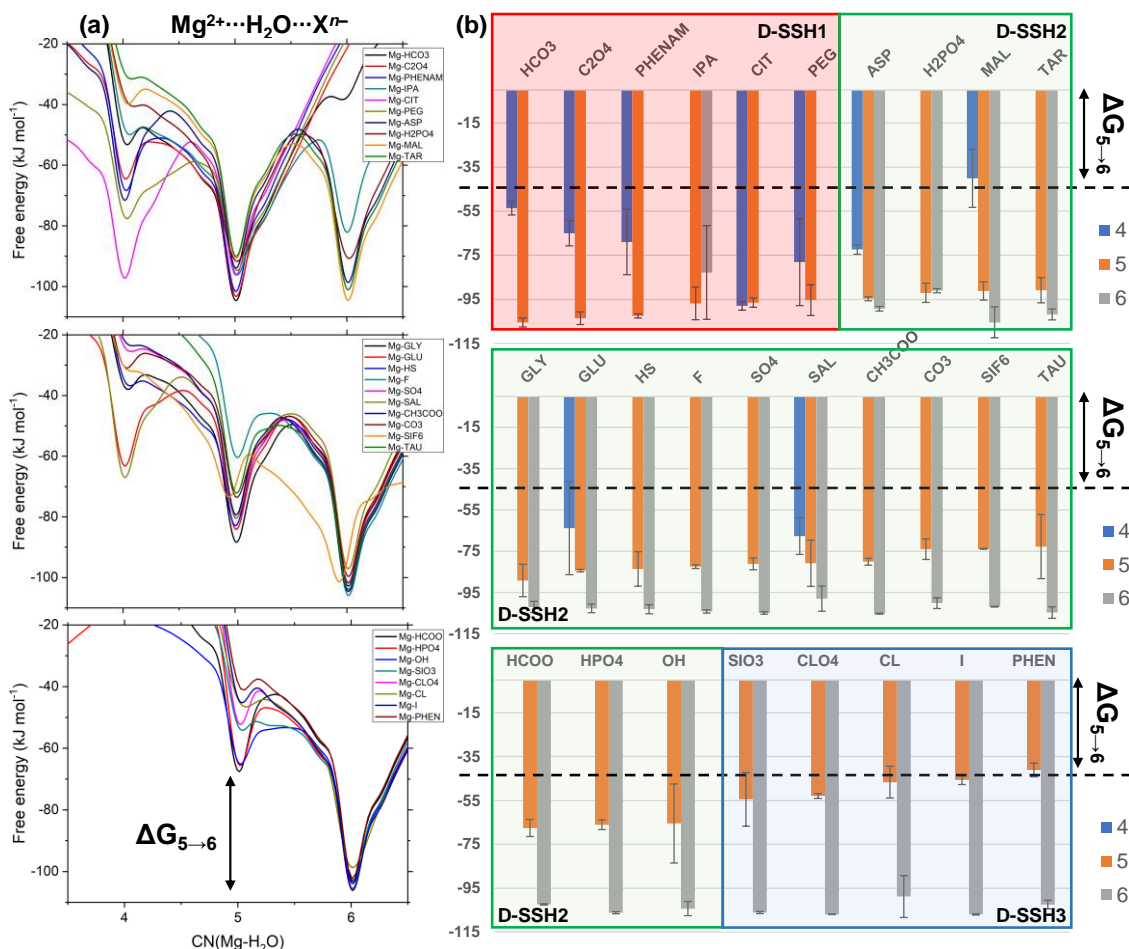
Figure 4. (a) Comparison of the free energy profiles as a function of the Mg^{2+}-H_2O coordination number, CN(Mg-H_2O), for solvated Mg^{2+} with a counterion in its second hydration shell (solvent-shared ion pairs, SSHIP). **(b)** Free energies of the $[Mg(H_2O)_4]^{2+}$, $[Mg(H_2O)_5]^{2+}$, and $[Mg(H_2O)_6]^{2+}$ states of Mg^{2+} in solutions containing additive anions (X^{n-}) with X^{n-} forming a SSHIP with Mg^{2+}.

D-CIP3: HCO3, HS, IPA, OH, CH3COO, GLU, ASP, SAL, PHEN, HCOO, F, SIO3, SIF6, TAU and GLY. All these ions stabilize the coordination five number. From these ions HS, HCO3, IPA, OH and CH3COO showed the higher propensity to stabilize the five-coordination state. A set of additives appeared to stabilise the six coordinated state, i.e. not able to replace any water molecule (TAU and GLY and SIF6) although they showed competitive energy release on stabilizing the five-coordination number. This implies that these additives can form a non-stable contact ion pair which can spontaneously detaches from the Mg species.

D-CIP4: CLO4, CL, NO3, I. These ions have a distinct preference to only stabilize the six hydration state, $Mg(H_2O)_6^{2+}$, without having any ability to for contact ion paring with Mg^{2+}.

We have examined in **Table 3** the additives considered in the present study to promote Mg^{2+} dehydration, without being competitive to the formation of the building unit of magnesite, $Mg^{2+}\cdots CO_3^{2-}$ CIP, based on the following three criteria. **Criteria 1**: competition between X^{n-} and CO_3^{2-} ion pairing with Mg^{2+}; a solution additive should preferentially form $Mg^{2+}\cdots H_2O\cdots X^{n-}$ SSHIPs or $Mg^{2+}\cdots X^{n-}$ CIPs less stable than $Mg^{2+}\cdots CO_3^{2-}$. **Criteria 2:** stabilization of undercoordinated Mg^{2+} states: X^{n-} in the second coordination shell of Mg^{2+}, $Mg^{2+}\cdots H_2O\cdots X^{n-}$ SSHIP, should stabilize undercoordinated $Mg(H_2O)_5^{2+}$ compared with the hexa-aquo $Mg(H_2O)_6^{2+}$ complex. **Criteria 3:** stabilization of low hydration $Mg(X)(H_2O)_m^{2-n}$ states; X^{n-}directly coordinated to Mg^{2+}, $Mg^{2+}\cdots X^{n-}$

10

CIP, should stabilize $Mg(X)(H_2O)_3^{2-n}$ and $Mg(X)(H_2O)_4^{2-n}$ complexes. The reported analysis provides a fundamental understanding of the role of solution additives in the Mg^{2+} dehydration process and could help ractionalize experimental observation of the effect of solvation environments on the growth of Mg-carbonates. A more detailed analysis based on the IP, D-SSH and S-CIP classification has also been reported in **Table S2** of Supporting Information.

Table 3. Summary of the ability of solution additive anions to promote Mg^{2+} dehydration based on the following criteria. **Criteria 1:** Mg^{2+} interaction with X^{n-}: competition with $Mg^{2+}\cdots CO_3^{2-}$ pairing; solution additive should forms $Mg^{2+}\cdots H_2O\cdots X^{n-}$ SSHIP or $Mg^{2+}\cdots X^{n-}$ CIP should be less stable than $Mg^{2+}\cdots CO_3^{2-}$; **Criteria 2:** Stabilization of undercoordinated Mg^{2+} states: influence of counterions on the Mg^{2+} dehydration kinetics; $Mg^{2+}\cdots H_2O\cdots X^{n-}$ SSHIP should stabilize undercoordinated $Mg(H_2O)_5^{2+}$ compared with the hexa-aquo $Mg(H_2O)_6^{2+}$ complex; **Criteria 3:** Stabilization of low hydration $Mg(X)(H_2O)_m^{2-n}$ number states: for $Mg^{2+}\cdots X^{n-}$ CIP the $Mg(X)(H_2O)_3^{2-n}$ and $Mg(X)(H_2O)_4^{2-n}$ complexes should be the most stable in solution.

	Criteria 1	Criteria 2	Criteria 3
CH3COO	√	√	
HS	√	√	
HCO3	√	√	
CIT	√	√	√
PHENAM	√	√	√
C2O4	√	√	√
SO4	√	√	√
MAL	√	√	√
GLU	√	√	
GLY	√	√	
SAL	√	√	
H2PO4	√	√	√
ASP	√	√	
HCOO	√	√	
TAU	√	√	
F	√	√	
PEG		√	
IPA		√	
HPO4		√	√
OH		√	
SIO3		√	
PHEN		√	
SIF6		√	
CLO4		√	
Cl			
I			
NO3			
PO4			√
TAR			√

We have further investigated the effect of selected additives on the formation of prenucleation MgCO$_3$ clusters by conducting extensive MD simulations (> 50 ns) of three aqueous electrolyte solutions containing 1 mol dm^{-3}

11
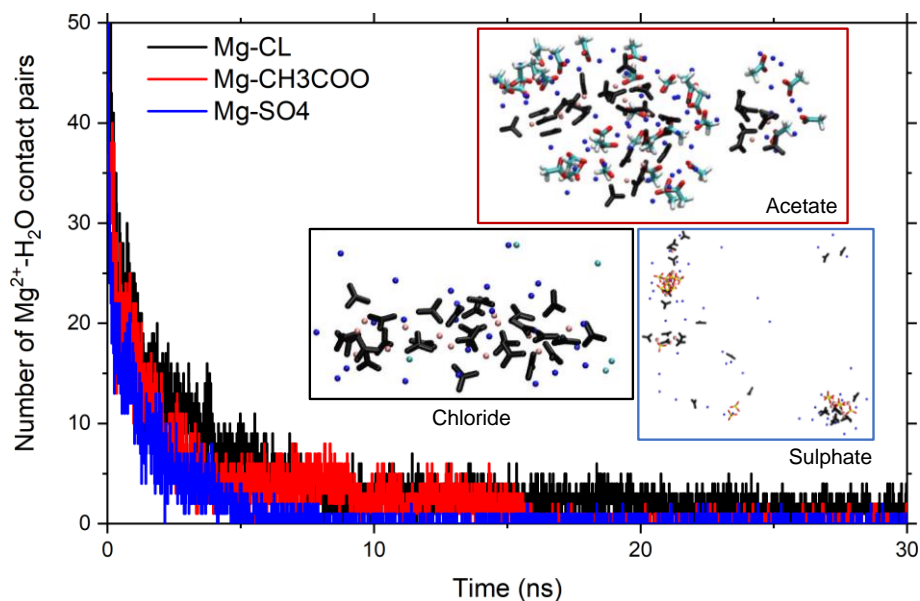
Figure 5. Progressive contacts pairs of Mg^{2+} with the oxygen atom of the water molecules. Snapshots of $MgCO_3$ clusters forming in the presence of acetate, chloride, and sulphate ions.

of Na_2CO_3 and 0.5 mol.dm^{-3} of $MgCl_2$, $MgSO_4$ and $Mg(CH_3COO)_2$, respectively. These solutions were generated by ensuring that each Mg^{2+} ion in the first configuration of the simulation was fully hydrated. **Fig. 5** shows the number of $Mg^{2+}\cdots H_2O$ pairs as a function of the simulation time, which decreases rapidly indicating that within the first few ns there is complete dehydration of Mg^{2+} and formation of the first $MgCO_3$ clusters, a crystallization event that which would be very difficult to observe using experimental techniques. The tendency of dehydration and consequent $MgCO_3$ aggregation follows the trend $SO_4^{2-} > CH_3COO^- > Cl^-$ and agrees with what observed from meta-dynamics calculations of the Mg^{2+} dehydration process.

4. Conclusions

The precipitation of anhydrous $MgCO_3$, a route for the storage and utilization of carbon dioxide, is a slow process which has been linked to the to the very strong $Mg^{2+}\cdots H_2O$ interaction, which raises the barrier of Mg^{2+} dehydration. Solution environments could be highly influential on the molecular processes controlling the kinetics of the early stages of magnesite formation from solution. The difficulty of experimentally tracking the early stages of $MgCO_3$ nucleation can be redressed by computational insights into the structural & energetic contributions of the nucleation sites and solution additives. In this study, we have used a combination of atomistic simulations, based on molecular dynamics and enhanced sampling (metadynamics) techniques, to investigate the effect of thirty additive anions, ranging from simple halides to more complex molecules, on the first two stages of $MgCO_3$ nucleation: Mg^{2+} dehydration and $Mg^{2+}\cdots CO_3^{2-}$ pairing. Based on the calculation of the thermodynamic stability of solvent shared ion pairs, $Mg^{2+}\cdots H_2O\cdots X^{n-}$, and contact ion pairs, $Mg^{2+}\cdots X^{n-}$, and the stabilization of undercoordinated hydrated Mg^{2+} states, we have classified additives based on theoir ability to promote Mg^{2+} dehydration, without being inhibiting the formation of the building unit of magnesite, the $Mg^{2+}\cdots CO_3^{2-}$ contact ion pair. Further simulations of the formation of $MgCO_3$ clusters in the presence of chlorine, acetate, and sulphate ions show the effect of the additives on the aggregation process as well. The findings of our study may provide

guidance to rationalize the effect of solution composition and reveal conditions of solution composition catalysing

300   magnesite formation.

Acknowledgements

References

315   (1)   Mission Innovation. 2017. Report of the carbon capture, utilization and storage experts' workshop. Houston. Available at: https://www.energy.gov/sites/prod/files/2018/05/f51/Accelerating Breakthrough Innovation in Carbon Capture%2C Utilization%2C and Storage_0.pdf (Accessed July 21, 2021).

(2)   U.S. Geological Survey, 2017, Mineral commodity summaries 2017: U.S. Geological Survey, 202 p., https://doi.org/10.3133/70180197.

320   (3)   Imbabi, M. S.; Carrigan, C.; McKenna, S. Trends and Developments in Green Cement and Concrete Technology. *Int. J. Sustain. Built Environ.* **2012**, *1* (2), 194–216.

(4)   Mazzotti, M.; Carlos, J.; Allam, R.; Lackner, K. S.; Meunier, F.; Rubin, E. M.; Sanchez, J. C.; Yogo, K.; Zevenhoven, R. Mineral Carbonation and Industrial Uses of Carbon Dioxide. *IPCC Spec. Rep. Carbon dioxide Capture Storage* **2005**, 319–338.

325   (5)   Giammar, D. E.; Bruant Jr., R. G.; Peters, C. A. Forsterite Dissolution and Magnesite Precipitation at Conditions Relevant for Deep Saline Aquifer Storage and Sequestration of Carbon Dioxide. *Chem. Geol.* **2005**, *217* (3–4), 257–276.

(6)   Swanson, E. J.; Fricker, K. J.; Sun, M.; Park, A.-H. A. Directed Precipitation of Hydrated and Anhydrous Magnesium Carbonates for Carbon Storage. *Phys. Chem. Chem. Phys.* **2014**, *16* (42), 23440–23450.

330   (7)   Prigiobbe, V.; Hänchen, M.; Werner, M.; Baciocchi, R.; Mazzotti, M. Mineral Carbonation Process for

CO$_2$ Sequestration. *Energy Procedia* **2009**, *1* (1), 4885–4890.

(8)   Di Tommaso, D.; de Leeuw, N. H. The Onset of Calcium Carbonate Nucleation: A Density Functional Theory Molecular Dynamics and Hybrid Microsolvation/Continuum Study. *J. Phys. Chem. B* **2008**, *112* (23), 6965–6975.

(9)   Zhang, X.; Alvarez-Lloret, P.; Chass, G. A.; Di Tommaso, D. Interatomic Potentials of Mg Ions in Aqueous Solutions: Structure and Dehydration Kinetics. *Eur. J. Mineral.* **2019**, *31* (2), 275–287.

(10)   McKenzie, J.; Vasconcelos, C. Dolomite Mountains and the Origin of the Dolomite Rock of Which They Mainly Consist: Historical Developments and New Perspectives. *Sedimentology* **2009**, *56* (1), 205–219.

(11)   King, H. E.; Satoh, H.; Tsukamoto, K.; Putnis, A. Nanoscale Observations of Magnesite Growth in Chloride- and Sulfate-Rich Solutions. *Environ. Sci. Technol.* **2013**, *47* (15), 8684–8691.

(12)   Berninger, U. N.; Jordan, G.; Lindner, M.; Reul, A.; Schott, J.; Oelkers, E. H. On the Effect of Aqueous Ca on Magnesite Growth - Insight into Trace Element Inhibition of Carbonate Mineral Precipitation. *Geochim. Cosmochim. Acta* **2016**, *178*, 195–209.

(13)   Power, I. M.; Kenward, P. A.; Dipple, G. M.; Raudsepp, M. Room Temperature Magnesite Precipitation. *Cryst. Growth Des.* **2017**, *17* (11), 5652–5659.

(14)   Song, X.; Dai, C.; Chen, G.; Dong, C.; Yu, J. Effect of Alcohol on the Crystallization Process of MgCO3·3H2O: An Experimental and Molecular Dynamics Simulation Study. *Energy Sources, Part A Recover. Util. Environ. Eff.* **2020**, *42* (9), 1118–1131.

(15)   Power, I. M.; Harrison, A. L.; Dipple, G. M.; Southam, G. Carbon Sequestration via Carbonic Anhydrase Facilitated Magnesium Carbonate Precipitation. *Int. J. Greenh. Gas Control* **2013**, *16*, 145–155.

(16)   Hem, B. J. D. *Study and Interpretation of the Chemical Characteristics of Natural Water*; 1985.

(17)   Tao, J.; Zhou, D.; Zhang, Z.; Xu, X.; Tang, R. Magnesium-Aspartate-Based Crystallization Switch Inspired from Shell Molt of Crustacean. *Proc. Natl. Acad. Sci.* **2009**, *106* (52), 22096-22101.

(18)   Bielak, K.; Różycka, M. O.; Zoglowek, A.; Ożyhar, A.; Dobryszycki, P. Counter-Diffusion System as an in Vitro Model in the Investigation of Proteins Involved in the Formation of Calcium Carbonate Biominerals. *Cryst. Growth Des.* **2021**, *21* (3), 1389–1400.

(19)   Kitadai, N.; Yokoyama, T.; Nakashima, S. Hydration–Dehydration Interactions between Glycine and Anhydrous Salts: Implications for a Chemical Evolution of Life. *Geochim. Cosmochim. Acta* **2011**, *75* (21), 6285–6299.

(20)   Khotyanovich, O. E.; Kuz'menkov, M. I. Technology of Magnesium Hexafluorosilicate Production. *Russ. J. Appl. Chem.* **2007**, *80* (11), 1977–1983.

(21)   Anthony, R.A. Bideaux, K.W. Bladh and M.C. Nicois **1997**. Handbook of Mineralogy. Volume III. Halides, Hydroxides, Oxides. Xi + 628 Pp. Tucson: Mineral Data Publishing. ISBN 0 9622097 2 4.

(22)   Van Der Spoel, D.; Lindahl, E.; Hess, B.; Groenhof, G.; Mark, A. E.; Berendsen, H. J. C. GROMACS:

14

365   Fast, Flexible, and Free. *J. Comput. Chem.* **2005**, *26* (16), 1701–1718.

(23)   Barducci, A.; Bussi, G.; Parrinello, M. Well-Tempered Metadynamics: A Smoothly Converging and Tunable Free-Energy Method. *Phys. Rev. Lett.* **2008**, *100* (2), 20603.

(24)   Tribello, G. A.; Bonomi, M.; Branduardi, D.; Camilloni, C.; Bussi, G. PLUMED 2: New Feathers for an Old Bird. *Comput. Phys. Commun.* **2014**, *185* (2), 604–613.

370   (25)   Raiteri, P.; Demichelis, R.; Gale, J. D. Thermodynamically Consistent Force Field for Molecular Dynamics Simulations of Alkaline-Earth Carbonates and Their Aqueous Speciation. *J. Phys. Chem. C* **2015**, *119* (43), 24447–24458.

(26)   Raiteri, P.; Demichelis, R.; Gale, J. D. Thermodynamically Consistent Force Field for Molecular Dynamics Simulations of Alkaline-Earth Carbonates and Their Aqueous Speciation. *J. Phys. Chem. C* 375   **2015**, *119* (43), 24447–24458.

(27)   Wang, J., Wang, W., Kollman P. A.; Case, Automatic Atom Type and Bond Type Perception in Molecular Mechanical Calculations. *J. Mol. Graph. Model.* **2006**, *25*, 247260.

(28)   Wang, J.; Cieplak, P.; Kollman, P. A. How Well Does a Restrained Electrostatic Potential (RESP) Model Perform in Calculating Conformational Energies of Organic and Biological Molecules? *J. Comput. Chem.* 380   **2000**, *21*, 1049.

(29)   Berendsen, H. J. C.; Grigera, J. R.; Straatsma, T. P. The Missing Term in Effective Pair Potentials. *J. Phys. Chem.* **1987**, *91* (24), 6269–6271.

(30)   Cornell, W. D.; Cieplak, P.; Bayly, C. I.; Gould, I. R.; Merz, K. M.; Ferguson, D. M.; Spellmeyer, D. C.; Fox. T.; Caldwell, J. W.; Kollman, P. A. Second Generation Force Field for the Simulation of Proteins, 385   Nucleic Acids, and Organic Molecules. *J. Am. Chem. Soc.* **1995**, *117* (19), 5179–5197.

(31)   Frisch, M. J.; Trucks, G. W.; Schlegel, H. B.; Scuseria, G. E.; Robb, M. A.; Cheeseman, J. R.; Scalmani, G.; Barone, V.; Mennucci, B.; Petersson, G. A.; Nakatsuji, H.; Caricato, M.; Li, X.; Hratchian, H. P.; Izmaylov, A. F.; Bloino, J.; Zheng, G.; Sonnenberg, J. L.; Had, D. J. Gaussian 09, Revision E.01. In *Gaussian, Inc Wallingford CT*; 2009.

390   (32)   Ruiz-Agudo, E.; Urosevic, M.; Putnis, C. V.; Rodríguez-Navarro, C.; Cardell, C.; Putnis, A. Ion-Specific Effects on the Kinetics of Mineral Dissolution. *Chem. Geol.* **2011**, *281* (3–4), 364–371.

(33)   Fennell, C. J.; Bizjak, A.; Vlachy, V.; Dill, K. A. Ion Pairing in Molecular Simulations of Aqueous Alkali Halide Solutions. *J. Phys. Chem. B* **2009**, *113*, 6782–6791.

(34)   Di Tommaso, D.; Ruiz-Agudo, E.; De Leeuw, N. H.; Putnis, A.; Putnis, C. V. Modelling the Effects of 395   Salt Solutions on the Hydration of Calcium Ions. *Phys. Chem. Chem. Phys.* **2014**, *16* (17), 7772–7785.

(35)   Friesen, S.; Hefter, G.; Buchner, R. Cation Hydration and Ion Pairing in Aqueous Solutions of MgCl 2 and CaCl 2. *J. Phys. Chem. B* **2019**, *123* (4), 891–900.

(36)   Rudolph, W. W.; Irmer, G.; Hefter, G. T. Raman Spectroscopic Investigation of Speciation in

MgSO4(Aq). *Phys. Chem. Chem. Phys.* **2003**, *5* (23), 5253–5261.

(37)   Qian, Z.; Feng, H.; Wang, C.; Chen, J. Theoretical Investigation of the Dissociative Interchange (Id) Mechanism for Water Exchange on Magnesium(II) in Aqueous Solution. *Inorganica Chim. Acta* **2010**, *363* (13), 3627–3631.

(38)   Woodley, S. M.; Catlow, C. R. A. High Performance Computing in the Chemistry of Materials. *Phys. Chem. Chem. Phys.* **2014**, *16* (39), 21001.

(39)   Roy, S.; Baer, M. D.; Mundy, C. J.; Schenter, G. K. Reaction Rate Theory in Coordination Number Space: An Application to Ion Solvation. *J. Phys. Chem. C* **2016**, *120* (14), 7597–7605.

(40)   Mergelsberg, S. T.; Kerisit, S. N.; Ilton, E. S.; Qafoku, O.; Thompson, C. J.; Loring, J. S. Low Temperature and Limited Water Activity Reveal a Pathway to Magnesiteviaamorphous Magnesium Carbonate. *Chem. Commun.* **2020**, *56* (81), 12154–12157.

(41)   Miller, Q. R. S.; Kaszuba, J. P.; Schaef, H. T.; Bowden, M. E.; McGrail, B. P.; Rosso, K. M. Anomalously Low Activation Energy of Nanoconfined MgCO3 Precipitation. *Chem. Commun.* **2019**, *55* (48), 6835–6837.

(42)   Power, I. M.; Kenward, P. A.; Dipple, G. M.; Raudsepp, M. Room Temperature Magnesite Precipitation. *Cryst. Growth Des.* **2017**, *17* (11), 5652–5659.